Journal of Inorganic Biochemistry 112 (2012) 49–58

Contents lists available at SciVerse ScienceDirect

Journal of Inorganic Biochemistry

journal homepage: www.elsevier.com/locate/jinorgbio

Development of metal-chelating inhibitors for the Class II fructose 1,6-bisphosphate (FBP) aldolase[☆]

Geneviève Labbé, Anthony P. Krismanich, Sarah de Groot, Timothy Rasmusson, Muhong Shang, Matthew D.R. Brown, Gary I. Dmitrienko, J. Guy Guillemette [*]

Department of Chemistry, University of Waterloo, 200 University Ave. W, Waterloo, ON, Canada N2L 3G1

ARTICLE INFO

Article history:
Received 27 October 2011
Received in revised form 26 February 2012
Accepted 26 February 2012
Available online 10 March 2012

Keywords:
FBP aldolase
Competitive slow-binding inhibitors

ABSTRACT

It has long been suggested that the essential and ubiquitous enzyme fructose 1,6-bisphosphate (FBP) aldolase could be a good drug target against bacteria and fungi, since lower organisms possess a metal-dependant (Class II) FBP aldolase, as opposed to higher organisms which possess a Schiff-base forming (Class I) FBP aldolase. We have tested the capacity of derivatives of the metal-chelating compound dipicolinic acid (DPA), as well a thiol-containing compound, to inhibit purified recombinant Class II FBP aldolases from *Mycobacterium tuberculosis*, *Pseudomonas aeruginosa*, *Bacillus cereus*, *Bacillus anthracis*, and from the Rice Blast causative agent *Magnaporthe grisea.* The aldolase from *M. tuberculosis* was the most sensitive to the metal-chelating inhibitors, with an IC_{50} of 5.2 μM with 2,3-dimercaptopropanesulfonate (DMPS) and 28 μM with DPA. DMPS and the synthesized inhibitor 6-(phosphonomethyl)picolinic acid inhibited the enzyme in a time-dependent, competitive fashion, with second order rate constants of 273 and 270 $M^{-1}\,s^{-1}$ respectively for the binding of these compounds to the *M. tuberculosis* aldolase's active site in the presence of the substrate FBP (K_M 27.9 μM). The most potent first generation inhibitors were modeled into the active site of the *M. tuberculosis* aldolase structure, with results indicating that the metal chelators tested cannot bind the catalytic zinc in a bidentate fashion while it remains in its catalytic location, and that most enzyme-ligand interactions involve the phosphate binding pocket residues.

© 2012 Elsevier Inc. All rights reserved.

1. Introduction

The metal-dependant Class II fructose 1,6-bisphosphate (FBP) aldolase has been proposed to be a good antimicrobial target because it is present in many plant and human pathogens, but not in animals or plants [1]. FBP aldolases (E.C. 4.1.2.13) catalyze the reversible aldol condensation of dihydroxyacetonephosphate (DHAP) and glyceraldehyde 3-phosphate (GAP) in glycolysis, gluconeogenesis, and the Calvin cycle. The Class I aldolase forms a Schiff base using an active site lysine residue with the keto group of the substrate; whereas the Class II enzyme uses a divalent metal ion as an electron sink to stabilize the carbanion formed on the 3rd carbon of the substrate. Attempts to disrupt the Class II FBP aldolase genes from *Mycobacterium tuberculosis*, *Escherichia coli*, *Streptomyces galbus*, *Bacillus subtilis*, *Pseudomonas aeruginosa*, *Streptococcus pneumoniae*, *Saccharomyces cerevisiae*, and *Candida albicans* by insertion or deletion mutagenesis have been unsuccessful, thereby suggesting that the Class II FBP aldolases are essential for the viability of these organisms [2–13]. The essential role of the Class II FBP aldolase for the growth of *M. tuberculosis* on glucose or gluconeogenic substrates *in vitro* has been confirmed recently by knock-out experiments, with a clear demonstration that the chromosomal copy of the Class II FBP aldolase can be deleted only in the presence of a rescue copy of the gene in that organism [14]. The Class II FBP aldolase from *M. tuberculosis* was shown to be strongly expressed in the granulomatous lung tissues of infected mice and guinea pigs [14].

The glycolysis/gluconeogenesis pathway, at the core of the central metabolism of all cells, may therefore be a drug target. In this pathway, we are targeting an essential metabolic enzyme, Class II FBP aldolase, which is not found in eukaryotic cells. We propose that the blockage of this central pathway will inhibit the growth of the cell by shutting down its core metabolism and all synthetic pathways due to the accumulation of phosphorylated metabolites [15–17]. This will result in the inhibition of ribosomal RNA transcription and effectively prevent ribosomes from being synthesized.

In this investigation, a series of commercially available and synthetic compounds were screened to determine starting points for the rational design of ligands for this class of enzyme. A few known inhibitors of Class II aldolases, all derivatives of the reaction intermediate analogue phosphoglycolohydroxamic acid (PGH), have been reported [1,18–21]. Unfortunately, it has been found that there are significant side-effects associated with drugs bearing hydroxamic

---

[☆] Inhibitor synthesis was carried out by A. K., T. R., M. R., and M. B. under the direction of G. I. D.; protein preparations and kinetic studies were carried out by G. L. and S. G. under the direction of J. G. G.; molecular modeling was performed by G. L. and G. I. D. The manuscript was written by G. L., A. K., G. I. D. and J. G. G.

[*] Corresponding author at. Tel.: +1 519 888 4567x35954; fax: +1 519 746 0435.
E-mail address: jguillem@uwaterloo.ca (J.G. Guillemette).

0162-0134/$ – see front matter © 2012 Elsevier Inc. All rights reserved.
doi:10.1016/j.jinorgbio.2012.02.032

acid functions [22]. As a result, we have chosen to approach the discovery of novel drug candidates that specifically inhibit the Class II aldolase over the mammalian Class I aldolase and that incorporate other metal-binding moieties such as thiols and carboxylates. Ultimately the synthesized compounds should be specific inhibitors of the Class II enzymes and form a stable ternary complex with the enzyme and the active site zinc, instead of promoting the release of the catalytic zinc ion (non-complexing inhibition).

Several derivatives of the metal chelator dipicolinic acid (DPA) were synthesized and evaluated as FBP aldolase inhibitors. This compound was chosen as the starting point for the synthesis of Class II FBP aldolase inhibitors in part because it was observed to have antifungal capabilities in our initial greenhouse tests (unpublished results). The antifungal and antibacterial capabilities of DPA were recently confirmed by an independent team [23]. DPA was also chosen as a starting point because it was shown to inhibit enzymes via a formation of a ternary complex (enzyme-zinc-DPA). For example, the removal of the zinc cofactor from bovine carbonic anhydrase (BCA), which is coordinated by three His residues and located in a deep narrow groove on the enzyme surface, was shown to occur through the formation of a ternary complex with DPA [24]; whereas the rate of the zinc removal from the enzyme by EDTA was shown to be governed by the spontaneous dissociation rate of the zinc-enzyme, with no evidence of ternary complex formation [25]. The inhibition of BCA by DPA was also found to be competitive with respect to the substrate bicarbonate [26]. Our goal is to produce DPA derivatives displaying improved competitive binding to the active site of FBP aldolase with respect to the substrate FBP.

In order to maximize our chances of finding an effective inhibitor against the microbial, metal-containing FBP aldolase (also called Class II FBP aldolase), we decided to study the enzymes from several microbes, including both human and plant pathogens. In this report, the results of studies of several commercial and newly synthesized metal-binding compounds will be described in terms of their capacity to inhibit the Class II FBP aldolases from human bacterial pathogens *M. tuberculosis*, *P. aeruginosa*, *B. cereus*, *B. anthracis*, as well as from the ascomycete fungus *M. grisea*, causative agent of rice blast. The Class I FBP aldolase from rabbit muscle was used as a negative control to assess the specificity of the compounds for the Class II enzymes. The inhibition kinetics of the most potent compounds with the aldolase from *M. tuberculosis* and the stability of the enzyme-inhibitor complexes will be discussed. The crystallographic structure of the *M. tuberculosis* Class II FBP aldolase was recently determined with its substrates DHAP and G3P bound to the active site [5]. The compounds tested here were modeled into the structure of the *M. tuberculosis* FBP aldolase. Suggestions as to how such inhibitors might be modified to lead to improved potency are provided.

2. Materials and methods

2.1. Inhibition screens

All buffers and solutions were prepared with deionized Milli Q water (Millipore, Bedford, MA). The rabbit muscle Class I aldolase was purchased from Sigma-Aldrich (Mississauga, ON). The Class II FBP aldolases were purified as described previously [27–29]. The synthesis of the inhibitors is summarized in Scheme 1, and is described in Appendix A (Supplementary material). The structure of each of the synthetic inhibitors was established by ^{1}H NMR (300 MHz), ^{13}C NMR (75 MHz), and mass spectrometry, and the purity of the compounds was assessed to be greater than 95% by examination of the ^{1}H NMR spectra (Appendix A).

The standard assay mixture (final volume 100 μL) contained the FBP aldolase (0.003 to 0.020 U/mL), 0.3 mM NADH, 0.2 U/mL of rabbit muscle α-glycerophosphate dehydrogenase, 2.25 U/mL of rabbit muscle triose phosphate isomerase, 0.2 mg/mL bovine serum albumin (BSA), 100 mM potassium acetate, 5% v/v DMSO and 23.75 mM Hepes, pH 7.3. The molecules tested for inhibition (except compound **1**, shown in Scheme 1) were dissolved in 100% DMSO to produce 100 mM stock solutions. The compound **1** was dissolved directly in 50 mM Hepes, pH 7.3 to produce a 50 mM stock solution. EDTA was diluted in the Hepes buffer and tested in the same way but without DMSO. Assays were performed at 28 °C in quadruplicate in 96-well flat bottom polystyrene plates (Corning, NY). The reaction was initiated by the addition of FBP and monitored at 340 nm for 10 min on a 96-well plate reader (Spectramax 190, Molecular Devices, Sunnyvale, CA). With each enzyme studied, the FBP concentration employed was at least 10 times its K_M. The concentration of inhibitor was varied depending on the amount of inhibition recorded, but inhibitor concentrations of 20, 50, 75, 100, 200, 500, and 1000 μM were typically used to determine the IC_{50}s. The enzymes were pre-incubated with the inhibitor for 15 min in the coupled assay mixture prior to the addition of the substrate FBP. The compound **1** was freshly dissolved prior to the kinetic assays as it became less potent during long-term storage in solution. DPA and racemic 2,3-dimercaptopropane-1-sulfonate (DMPS) were purchased from Sigma-Aldrich (Mississauga, ON) and were freshly diluted in buffer prior to the assays.

2.2. Second order rate constants determination

The *M. tuberculosis* aldolase was used for these assays. Four replicates were done for each combination of substrate and inhibitor concentrations, and the reaction was monitored by absorbance readings every six seconds for 10 min using a coupled assay. The assays were started by addition of the enzyme to the substrate and inhibitor mixture, without pre-incubation of the enzyme with the inhibitor. The FBP concentrations used were 25, 40, 60, 80, 120, 200, and 500 μM. The inhibitor concentrations were 20, 50, 100 and 500 μM of DMPS and DPA; 20 and 50 μM of compound **1**; 50 and 100 μM of compound **7**, and 100 and 500 μM of EDTA. Eqs. (1) and (2) [30,31] presented below were fitted to each progress curve by non-linear regression using automatic outlier elimination (Rout coefficient Q set to 1% to exclude outliers, with no weighting) to obtain the apparent constants *k* or A using the GraphPad Prism software (GraphPad Software Inc, La Jolla, CA). A secondary plot of the apparent constant A multiplied by the inhibitor concentration versus the FBP concentration was then performed to obtain the on-rate constant k_{on} for each inhibitor (Eq. (3)), again using non-linear regression with GraphPad Prism as described above.

$$\text{(reversible inhibition)}\quad [\mathrm{P}]_{\mathrm{t}} = v_s \mathrm{t} + (v_0 - v_s)\left(1 - \mathrm{e}^{-kt}\right)/k \qquad (1)$$

$$\text{(irreversible inhibition)}\quad [\mathrm{P}]_{\mathrm{t}} = (v_0/[\mathrm{I}]\mathrm{A})\left(1 - \mathrm{e}^{-[\mathrm{I}]\mathrm{At}}\right) \qquad (2)$$

$$\text{When t approaches infinity, Equation 2 becomes : } [\mathrm{P}]_{\infty} = (v_0/[\mathrm{I}]\mathrm{A})$$

$$\text{(competitive irreversible inhibition)}\quad \mathrm{A} = k_{\mathrm{on}}/(1 + [\mathrm{S}]/K_{\mathrm{M}}) \qquad (3)$$

where $[P]_t$ is the concentration of product formed at time t, v_0 is the initial velocity, v_s is the end velocity, [I] is inhibitor concentration, [S] is the concentration of substrate, K_M is the Michaelis constant, and k_{on} is the second order rate constant for the binding of the competitive inhibitor (Fig. 1). The description of the apparent constants *k* and A depends on the type of inhibition (Competitive, Noncompetitive or Uncompetitive). Note that the constant *k* in Eq. (1) is equivalent to [I]A in Eq. (2).

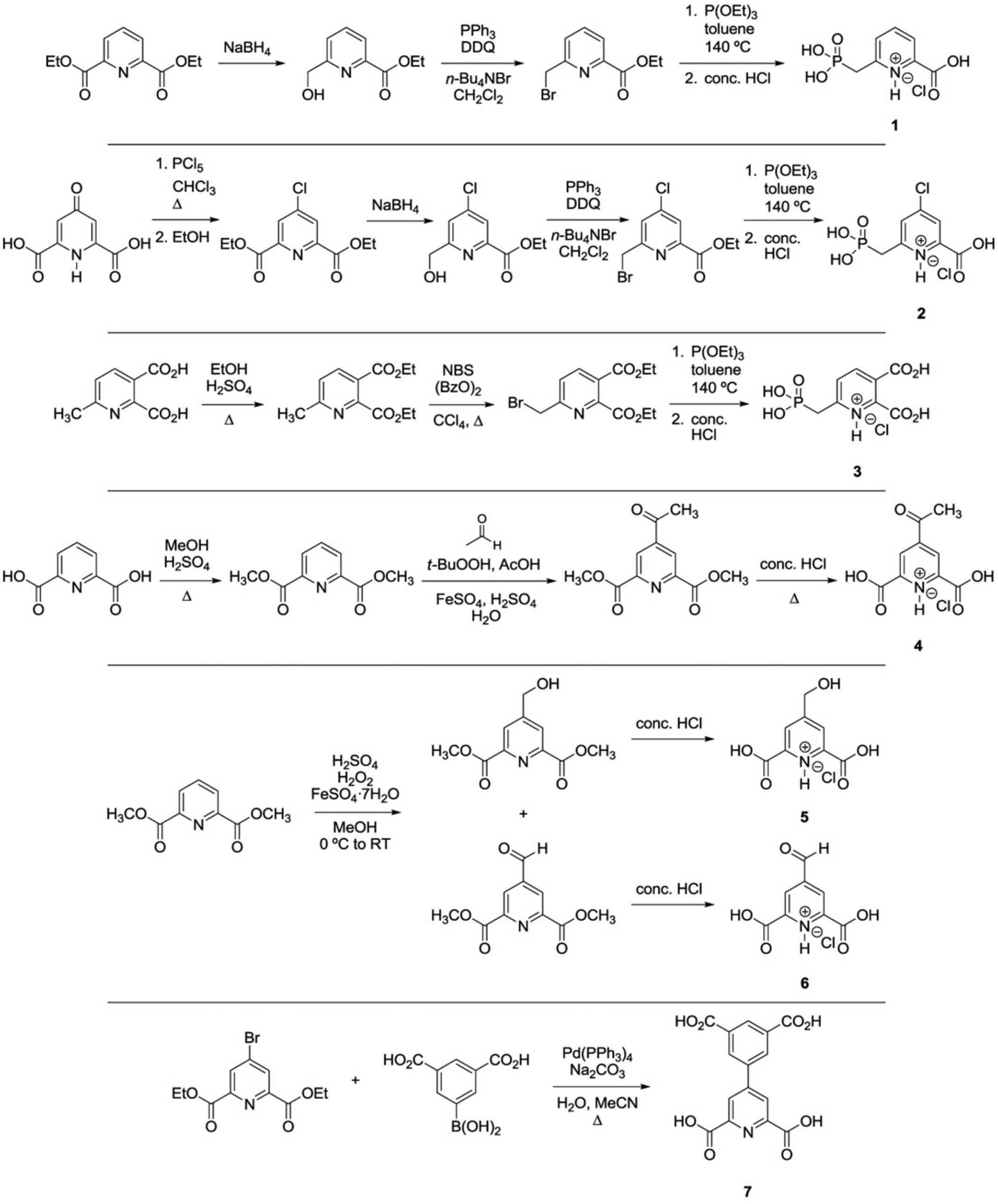
NaBH4
PPh3
DDQ
n-Bu4NBr
CH2Cl2
1. P(OEt)3
toluene
140 °C
2. conc. HCl
1
1. PCl5
CHCl3
Δ
2. EtOH
2
EtOH
H2SO4
NBS
(BzO)2
CCl4, Δ
3
MeOH
H2SO4
t-BuOOH, AcOH
FeSO4, H2SO4
H2O
conc. HCl
4
H2SO4
H2O2
FeSO4·7H2O
MeOH
0 °C to RT
5
6
Pd(PPh3)4
Na2CO3
H2O, MeCN
7

Scheme 1. The reaction sequences used in the synthesis of inhibitors 1–7.

2.3. Docking and molecular modeling

The inhibitors were docked into the active site of the *M. tuberculosis* aldolase using AutoDock Vina [32]. The substrates, the Na^+ ion, and the water molecules were deleted from a *M. tuberculosis* aldolase structure previously published (PDB ID: 3EKZ) [5] before the file was uploaded into AutoDockTools 1.5.4 [33] to calculate Gasteiger charges, merge the non-polar hydrogens and to assign AD4 atom types. The Zn parameters were modified to a radius of 0.87 Angstroms and a charge of +0.95e [34]. The dockings were done setting the enzyme (receptor) as being rigid, and the inhibitors flexible, as calculated in the AutoDock Tools quick setup option for ligands. The search was centered on the catalytic zinc coordinates with a box of 15×15×15 Å. The docking was done using the default search parameters of AutoDock Vina.

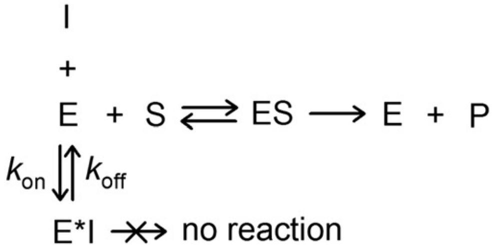
I
+
E + S ⇄ ES ⟶ E + P
k_on
k_off
E*I
no reaction

Fig. 1. Scheme of competitive reversible inhibition with associated rate constants.

Inhibitors containing phosphonate groups were also minimized in the *M. tuberculosis* monomer using the MMFF94 force field in Sybyl X1.3 (Tripos, St. Louis, MO). The compounds were positioned approximately in the space occupied by the substrates in the *M. tuberculosis* aldolase structure (PDB ID: 3EKZ), the files were merged, the substrates were deleted, and the whole enzyme-inhibitor complex was minimized employing the anneal function within Sybyl X1.3. Before minimization, it was necessary to modify the crystallographic structure so that the MMFF94 force field could assign proper atom types. The surface bound (second) zinc ion was deleted and all formal bonds to the metal ions (that were created automatically by the software when the pdb file was imported) were deleted. Atom types were modified to ensure that the lone pair electrons of the sp2- hybridized nitrogen atoms on the imidazole rings could make contact with the active site zinc ion. All water molecules in the pdb file were retained as was the sodium ion in the phosphate binding pocket. Since the crystal structure lacks structural information about the coordinates of certain stretches of amino acid residues, it was necessary to "cap" the C-termini of incompletely defined parts of the structure as primary amides to avoid computational problems caused by atoms with unspecified bonding arrangements. All hydrogen atoms were added and the ionization states of the inhibitors were modified before geometry optimization. In the case of DPA, both carboxylate groups were adjusted to be in an ionized state. For compound **1**, the carboxylate group was assumed to be ionized and the phosphonic acid group was assumed to be singly ionized such the anionic oxygen atom was oriented towards the sodium ion. In the case of DMPS, both the sulfonate group and the C-3 thiol group were adjusted to be singly ionized. Prior to initiating the energy minimization, the zinc ion, the sodium ion, manually docked inhibitor molecule, and all amino acid residues within a 10 Å radius were chosen as the "hot" region that was subjected to full geometry optimization. By default, an "interesting" region consisting of all amino acid residues within 12 Å of the "hot" region was defined and allowed to influence the geometry optimization in the "hot" region. A gradient convergence criterion = 0.05 kcal/mol*Å was employed to define geometry optimization. In each case, this criterion was achieved in approximately 20,000 iterations.

The images of the docked and minimized compounds were produced using PyMOL (DeLano Scientific LLC).

3. Results

3.1. Inhibition screens

Several Class II FBP aldolases previously characterized in our laboratory (those from *M. tuberculosis*, *M. grisea*, *P. aeruginosa* and *B. cereus*) were used in this study, in order to cover most of the evolutionary branches of the Class II aldolase phylogenetic tree [29]. The amino acid sequences of the FBP aldolases from *B. anthracis* and *B. cereus* are identical, therefore the results obtained for the *B. cereus* aldolase are applicable to the *B. anthracis* enzyme as well (the *B. cereus* strain ATCC 10987 was used in this study [29], and its amino acid sequence is the same as that of the aldolase from *B. anthracis* str. 'Ames Ancestor', whose structure was deposited in the Protein Data Bank recently (PDB ID: 3Q94)). Several potential inhibitory compounds were tested, including DPA derivatives (compounds **1**–**7**) (Scheme 1), in order to facilitate rational ligand design. The IC_{50} values of these inhibitors after 15 min of incubation were determined with the recombinant Class II FBP aldolases from the targeted microorganisms (Table 1). It is relevant to note that the presence of metal in the assay was found to significantly decrease the inhibitory capacity of the compounds, as less than 30% inhibition was observed after 15 min of incubation with 1 mM DPA or compound **1** for the *P. aeruginosa* aldolase in the presence of 0.7 mM $CoCl_2$, whereas the IC_{50} values in the absence of metal were 200 μM or less. An experiment was also performed to determine if the inhibition was reversible upon simple dilution in the assay mixture. The concentrated enzyme (100× compared to the assay concentration, or ~0.8 μM of *M. tuberculosis* aldolase) was incubated with 1 mM of the inhibitors EDTA and DPA, or 250 μM of compound **1** for 15 min, in the presence of 5% v/v DMSO. The enzyme was only ~60% inhibited by the compound **1** in these conditions. The aldolase was in contrast 100% inhibited by the pre-incubation with 1 mM EDTA and DPA under these conditions. The enzyme and inhibitor mixture was then diluted in the assay such that the inhibitor concentration was 10 μM (or 2.5 μM for compound **1**), and the reaction was immediately started by addition of FBP at a final concentration of 200 μM. The *M. tuberculosis* aldolase recovered its full activity in all cases but with DPA, where only ~5% of the activity was recovered.

According to the data presented in Table 1, the compounds tested appear to be generally no better than EDTA at inhibiting the Class II aldolases. However, these results were obtained after 15 min of pre-incubation in the absence of the substrate FBP. While performing similar experiments without pre-incubation with the inhibitory compounds, it was observed that the compounds were much less effective inhibitors when the substrate was present, pointing to a competitive mechanism. Some inhibitors were therefore assayed by varying both inhibitor and substrate concentration with and without the 15 min of pre-incubation of the enzyme with the inhibitor. However, the analysis showed that the competitive, uncompetitive, or mixed inhibition models did not fit the resulting data (Figure B1). The compounds in fact exhibited a time-dependent pattern of inhibition of the FBP cleavage reaction (see progress curves in the presence of various compounds in Fig. 2). In spite of being reversible upon simple dilution as described above, the inhibition did not appear reversible under the coupled assay conditions, as the reverse reaction was too slow to be detected. However the enzyme could be reactivated

Table 1
Summary of IC_{50} values for the inhibition of FBP aldolases with DPA derivatives.

Source organism	K_M (μM) for FBP[a]	IC_{50} (μM) obtained for each compound[b] (95% confidence interval)							
		DPA	1	2	3	4	5	6	EDTA
M. grisea	51 ± 1	79 (74–84)	78 (68–92)	960 (880–1,050)	1370 (1320–1420)	540 (480–630)	430 (400–470)	740 (710–770)	53 (45–66)
M. tuberculosis	27.9 ± 0.9	28 (24–36)	57 (54–62)	650 (590–710)	560 (520–600)	190 (160–230)	110[c] (91–140)	81 (61–120)	48 (44–53)
B. cereus	450 ± 10	150 (130–170)	78 (70–89)	1050 (950–1170)	1100 (990–1250)	N/I	170 (150–180)	740 (690–790)	8 (7–11)
P. aeruginosa	35 ± 2	95 (81–120)	130 (100–180)	> 1000	> 1500	> 1000	270 (230–340)	240 (200–300)	41 (37–45)
Rabbit muscle	5.1	N/I	N/I	N/I	–	N/I	680 (620–740)	N/I	N/I

N/I: no inhibition.
–: not determined.

[a] Values taken from [29] and [42].

[b] A one phase decay equation was fitted to the data by non-linear regression, and the 95% confidence interval for each IC_{50} value is indicated in brackets.

[c] The inhibition is affected by pH. This compound was also tested at a higher pH with the *M. tuberculosis* aldolase (assay at pH 8.0 instead of pH 7.3), and the IC_{50} was found to be ~500 μM in these conditions. The other compounds were not tested at different pH.

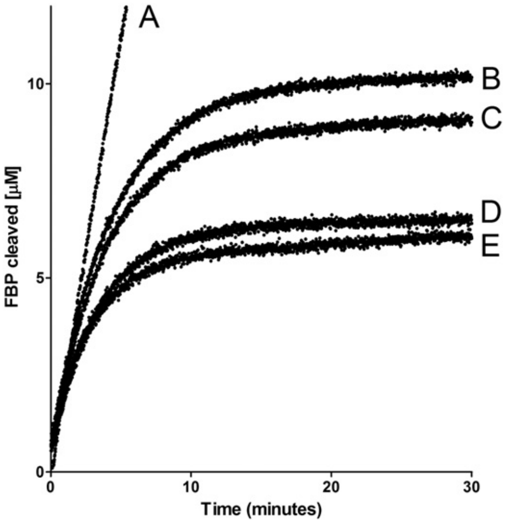

Fig. 2. Progress curves of FBP cleavage by *M. tuberculosis* Class II aldolase in the presence of different metal-chelating inhibitors. 3 nM of enzyme was used to start the reaction in the presence of 500 μM FBP and the following compounds: A) negative control (BSA, 3 μM); B) EDTA (5 mM); C) DMPS (500 μM); D) DPA (500 μM); and E) compound 7 (500 μM). After subtracting the background NADH oxidation from the data, the enzyme was calculated to be completely inactivated by the metal-chelating compounds after 20 min.

upon the addition of zinc to the assay mixture (Figure B2). The inhibition experiments were subsequently performed in the presence of substrate (no pre-incubation) and analyzed using a time-dependent inhibition model.

3.2. Inhibition mechanism determination

In order to determine the inhibition mechanism, we chose to use the enzyme from *M. tuberculosis*, as it generally was the most sensitive to the inhibitors during the initial screens (Table 1). Two additional compounds were tested: **7** and commercially available, thiol-containing compound DMPS. DMPS was investigated because it is already used for medical treatment in humans and animals, and it was also found to be an inhibitor of another zinc metalloenzyme *in vitro* [35]. The *M. tuberculosis* and *M. grisea* aldolases were inhibited strongly by DMPS, with IC_{50} values of 5.2 ± 0.4 μM and 31 ± 3 μM, respectively, while the rabbit muscle aldolase was not inhibited in the presence of 2 mM of this compound. Compound **7** was also tested with these enzymes, and inhibited the *M. tuberculosis* aldolase with an IC_{50} of 21 ± 3 μM and the *M. grisea* aldolase with an IC_{50} of 60 ± 4 μM. However, compound **7** also inhibited the rabbit muscle aldolase by 37% at a concentration of 2 mM. The most potent inhibitors from these screens (DPA, **1, 7,** and DMPS) were chosen for the inhibition mechanism studies, and EDTA was used for comparison.

The slow-binding inhibition progress curves can be fitted to Eq. (1) [30] (see Materials and methods section) in the case of reversible inhibition. The inhibition of the Class II aldolases was shown to be reversible upon the addition of metal, but the end velocity (v_s) obtained in our assay conditions is too low to be detected. This could be due to the background NADH oxidation which is relatively high in our coupled assay, and this masks any potential small residual aldolase activity. The observed enzyme inhibition is therefore not distinguishable from irreversible inactivation, so we will consider the end velocity (v_s) in Eq. (1) to be negligible and use instead Eq. (2) [31] (see Eq. (2) fitted to progress curves obtained in the presence of DMPS in Figure B3). The type of irreversible inhibition (Eq. (2)) can be distinguished by suitable plots of A and [S] [31]. In the case of competitive inhibition (Fig. 1), A is defined by Eq. (3), and thus a plot of 1/A versus [S] should give a straight line. Some of these plots obtained with the metal-chelating inhibitors are shown in Fig. 3. The results

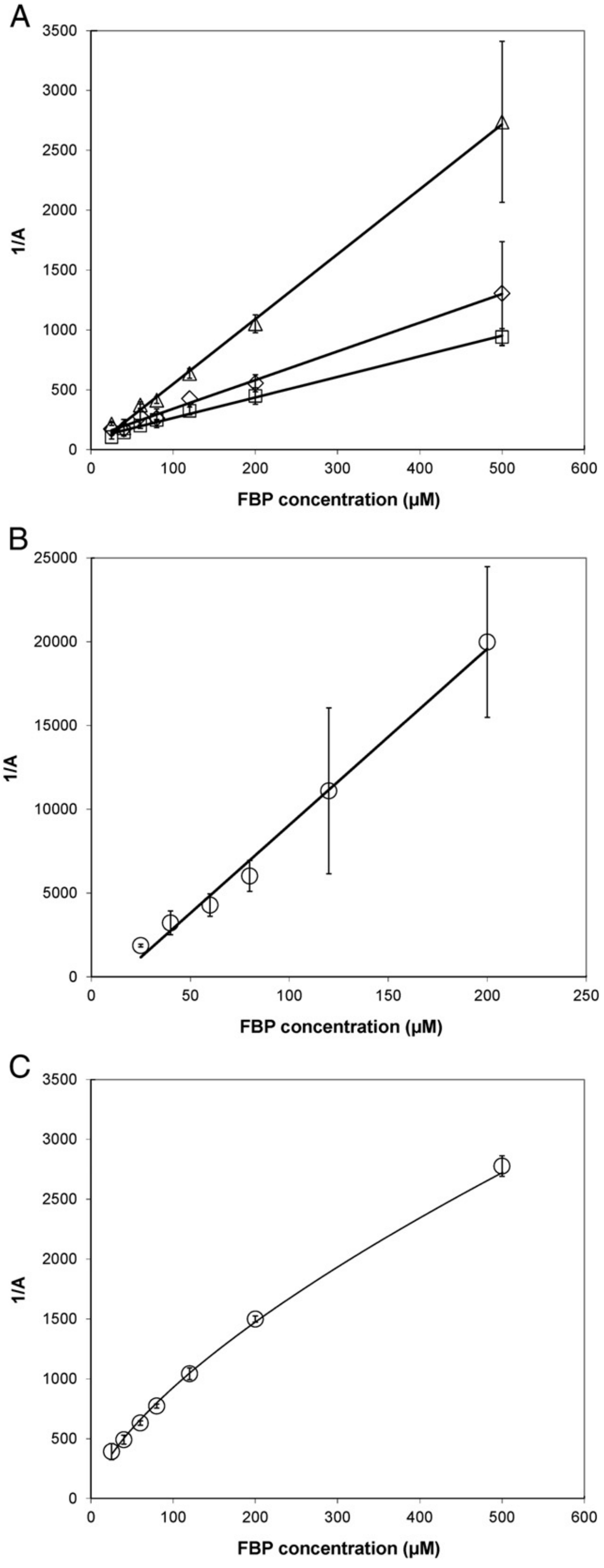

Fig. 3. Variation of the apparent rate of inhibition in function of the substrate concentration: Tsou's test for competitive irreversible inhibition. The apparent constant A was obtained by fitting Eq. (**2**) using non-linear regression to the progress curves obtained with the *M. tuberculosis* aldolase, in the presence of various concentrations of FBP and different inhibitors: panel A) 500 μM compound **1** (◊); 100 μM DMPS (□); 100 μM compound 7 (Δ); panel B) 500 μM EDTA (○); panel C) 500 μM DPA (○). Each point represents the average value of 4 replicate assays. Straight lines indicate that the inhibition is competitive with respect to the substrate FBP.

indicate that the (apparent) irreversible inactivation is competitive with the substrate for the inhibitors DMPS, EDTA, and compounds **1** and **7**. However, the high dispersion of the calculated constant A for these inhibitors at high substrate concentration means that non-linearity cannot be totally excluded, and these compounds may therefore not display purely competitive inhibition. In the case of DPA, the resulting plot is non-linear, indicating that this compound is a mixed inhibitor of the *M. tuberculosis* aldolase (Fig. 3C).

Since the inhibition appears irreversible under the assay conditions used, the apparent K_I cannot be determined for a one-step inhibition mechanism (Fig. 1), as it would represent the ratio of the forward and reverse inhibitor binding rate constants (k_{on}/k_{off}). The binding capacity of the most potent inhibitors will instead be compared using their second order binding rate constant k_{on} (Eq. (3), Fig. 1). The binding rate constant k_{on} was determined using the equation associated with a competitive inhibition model for all compounds for comparison purposes. The resulting plots are presented in Fig. 4. The k_{on} rate constants obtained with these inhibitors are presented in Table 2. The apparent inhibition constants obtained with DPA were also analyzed using a mixed inhibition equation (see Figure B4), yielding a $k_{on} = 73 \pm 4\ M^{-1}\ s^{-1}$, which is ~13% lower than the value presented in Table 2.

As can be seen from the results presented in Table 2, the inhibitors DMPS and compound **1** can inactivate the Class II FBP aldolase from *M. tuberculosis* ~20 times faster than EDTA, and ~3 times faster than DPA in the presence of the substrate FBP, whereas the inhibitor **7** can inactivate the enzyme almost 2 times faster than DPA in the presence of FBP. The apparent second order rate constants obtained for the irreversible reaction with these inhibitors are over 3 orders of magnitude lower than the second order rate constant determined for the FBP cleavage reaction for the *M. tuberculosis* aldolase ($k_{cat}/K_m = 1.08 \times 10^6\ M^{-1}\ s^{-1}$ [29]). It is therefore estimated that these inhibitors have an affinity for the active site ~3 orders of magnitude lower than the substrate FBP.

3.3. Molecular modeling

Initial efforts at exploring possible ways in which the pyridine carboxylate inhibitors bind to the active site of Class II aldolases were carried out by docking flexible inhibitor molecules to a rigid model of the protein. In each case, the docking exercise produced a model in which the inhibitor interacted with the active site region in a manner that is very different from the interaction of PGH, DHAP or the High Energy Intermediate (H.E.I.) with the enzyme (e.g. see a comparison of the H.E.I. binding mode and the docked structure of DPA determined using the rigid docking strategy in Fig. 5, panels A and B, and rigid docking results for other pyridine carboxylate inhibitors in Appendix C, Figure C1). The distances between H donors and acceptors from the ligands and the enzyme active site elements in all the modeled compounds are presented in Appendix C, Table C1.

It was concluded that the enzyme likely must undergo significant conformational alteration to accommodate the binding of the pyridine carboxylate inhibitors so that a rigid docking process might not be appropriate.

Thus construction of models by superimposition of the pyridine carboxylate inhibitors on the H.E.I. in the X-ray crystal structure of the complex ([5]) was undertaken. It proved possible to align a model of DPA such that one carboxylate group could interact with the zinc ion whereas the other carboxylate was in the vicinity of the phosphate binding site. Bad contacts between the inhibitor and the protein were then removed by geometry optimization with the Anneal functionality within Sybyl X1.3 using the MMFF94 molecular mechanics force field (see Materials and methods for more detail). Interestingly, even though such pyridine dicarboxylates are potentially capable of bidentate interaction with metal ions involving both the carboxylate anion and the pyridine nitrogen, none of the energy minimized complexes exhibited such interaction with the zinc ion (Fig. 5, panel C, and Appendix C, Figure C2, panels A–C). The pyridine ring is simply too large to permit such bidentate interaction in the Class II FBP aldolase active site.

The minimized models do suggest that the internuclear distance between the carboxylate groups of DPA is appropriate to allow significant monodentate binding between these two groups simultaneously with the zinc ion and the sodium ion in the phosphate binding site. The geometry optimization process did lead to significant alteration of the environment of the zinc ion compared to that observed in the X-ray crystal structure (PDB ID: 3EKZ) [5]. For example, some distortion of the orientation of the imidazole rings of the histidine residues around the zinc ion, as well as a new interaction of the carboxylate group of D95, was observed. Thus the zinc ion was predicted to be in a distorted trigonal bipyramidal environment.

In the case of the DPA analogues, **4**, **5**, and **6**, the additional steric bulk of the C-4 substituents appears to diminish the affinity for the FBP aldolase active site (Table 1, and Appendix C, Figure C2, panels A–C).

It proved possible to construct and geometry optimize a model of the pyridine carboxylate–phosphonate with the active site. In this model the phosphonate group is able to occupy the phosphate binding site with significant interaction with the sodium ion while the pyridine carboxylate group binds with the zinc ion (Fig. 5, panel D). The environment of the zinc ion was observed to be altered in a similar fashion to that observed in the energy minimized complex of DPA with the enzyme. In compounds **2** and **3** the pyridine substituents appear to lead to increased unfavorable interaction with the active site (Table 1 and Appendix C, Figure C2, panels D and E).

In the case of the pyridine dicarboxylate derivative, **7**, all attempts to construct an energy minimized active site bound model using a similar strategy were unsuccessful. The very large substituent at C-4 of the pyridine ring in this compound led to bad contacts with active site residues that could not be relieved in the molecular mechanics minimization without gross distortions of the inhibitor structure. Thus the relatively fast on rate observed for this compound is not explicable based on easy access or strong affinity for the H.E.I. binding site. One possibility is that this compound binds to the two metal ions via the carboxylate groups of the pyridine ring but with the pyridine ring and the large C-4 substituent external to the active site. In such a complex, the very large C-4 substituent might be capable of blocking access to the active site by the substrate leading to what would be competitive inhibition kinetically. Efforts to explore this possibility through X-ray crystallographic experiments are planned.

In the case of DMPS, which contains one chiral centre and which was analyzed as the racemic mixture, both the *R* and *S* enantiomers were docked manually in the active site as defined by the coordinates in the X-ray crystal structure of the *M. tuberculosis* FBP aldolase. In both cases a fully extended conformation was assumed as a starting point for the geometry optimization since only such a conformation allows interaction with both the zinc ion and the phosphate binding site. After energy minimization with the MMFF94 force field, the *R*-enantiomer was found to have a slightly closer contact with the zinc ion (C-3 thiolate ion to Zn^{2+} distance = 2.32 Å for the *S*-isomer versus 2.29 Å for the *R*-isomer) and with the sodium ion (sulfonate oxygen to Na^+ distance = 2.48 Å for the *S*-isomer versus 2.29 Å for the *R*-isomer) (Fig. 5, panels E and F; Table C1).

In the fully extended conformation, the two thiol/thiolate groups are in an anti-periplanar relationship (expected to be lower in energy) for the *S*-enantiomer but in a *gauche* relationship (expected to be higher in energy) for the *R*-enantiomer. Thus it is plausible that both enantiomers contribute significantly to the observed inhibition by racemic DMPS.

Although a bis-mercaptan, such as DMPS, has the potential to act as a bidentate metal ion ligand to the active site zinc ion, the short distance between the sulfonate group, that likely binds to the phosphate binding site, and the C-3 thiolate group allows only that sulfur

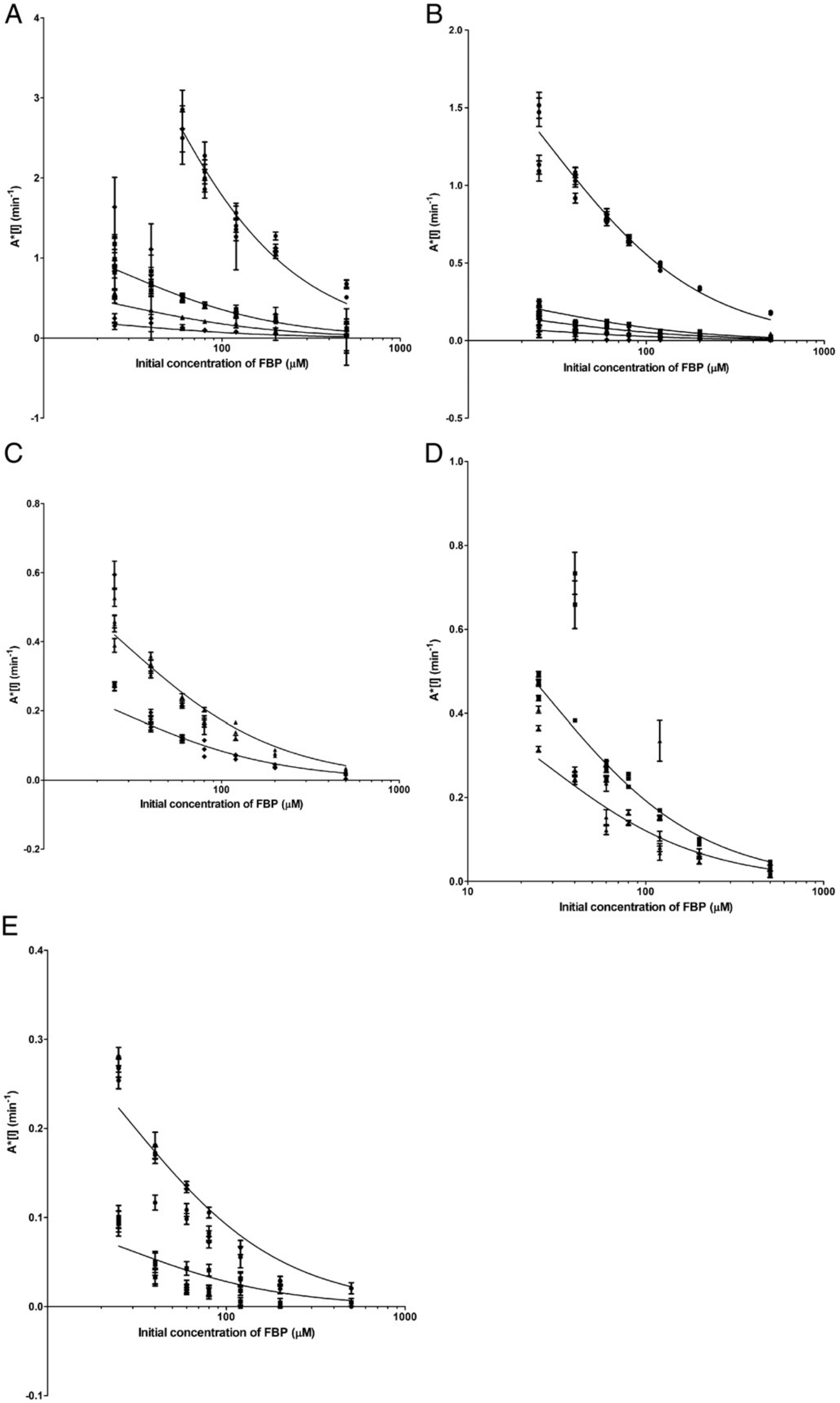

Fig. 4. Secondary plots of the apparent inhibition constants obtained with the *M. tuberculosis* aldolase in the presence of various inhibitors, as a function of the FBP concentration. The apparent inhibition constants (A*[I], represented by *k* in Eq. (1)) were obtained from 47 to 100 progress curves for each inhibitor, and are shown with their error bars representing the standard deviation. Eq. (3) defining the apparent constant A for competitive inhibition was fitted to the data by non-linear regression using the GraphPad Prism software. The equation was fitted independently to the data from each inhibitor concentration (shown as lines in each Panel), and the global parameters were also calculated. The global parameters calculated for each inhibitory compound are presented in Table 2. Panel A) DMPS; B) DPA; C) compound **1**; D) Compound 7; and E) EDTA. The concentrations of inhibitors used are 500 μM (●), 100 μM (■), 50 μM (▲), and 20 μM (◆).

Table 2
Second order rate constants for the binding of chelating inhibitors to the recombinant Class II aldolase from *M. tuberculosis*.
Each value is calculated from a secondary plot (Eq. (3)) using the apparent constant A (Eq. (2)) obtained for multiple assays done simultaneously in a microtiter plate in the presence of various concentrations of FBP and inhibitor.

Inhibitor	k_{on} M^{-1} s^{-1}	R^2 value of secondary plot
DPA	84 ± 1	0.9879
1	270 ± 6	0.9476
7	153 ± 3	0.9575
DMPS	273 ± 2	0.9941
EDTA	14 ± 1	0.8683

centre and not the C-2 sulfur centre to interact with the zinc ion. Current efforts in this group are aimed at creating synthetic analogues DMPS in which the spatial relationships among the two thiol groups and the sulfonate ion are such as to allow favorable binding to the phosphate binding site as well as more potent binding to the zinc ion in a bidentate fashion. Preliminary molecular modeling studies suggest that this may be feasible.

4. Discussion

Although the Class II FBP aldolases are potential targets for antimicrobial therapy and for the development of new fungicides, there have been few potent Class II FBP aldolase inhibitors reported in the literature. In order to create specific inhibitors for the metal-dependent Class II aldolases, compounds that have metal-chelating groups were tested. The results were compared with the general metal ion chelators, EDTA and DMPS. EDTA has an affinity for zinc which is $>10^4$ higher than that of DPA, based on the equilibrium constants for Zn^{2+} binding to these chelators [36]. The rate of enzyme inhibition by DPA and its derivatives is therefore expected to be faster than the rate of inhibition by EDTA only when the active site zinc is much more accessible to DPA compared to EDTA. In this study, inhibition by EDTA was used as a reference to evaluate the capability of DPA derivatives to compete with the aldolase substrate for access to active site zinc. This is considered to be in direct correlation with the DPA derivatives' affinity for the enzyme's active site.

The IC_{50} results show that in the absence of substrate, the active site zinc is accessible to both DPA and EDTA, based on the similar IC_{50} values obtained for these compounds for most Class II aldolases tested. The molecule 2,6-pyridinedicarboxylic acid (or dipicolinate, DPA) was the most potent inhibitor according to our initial compound screen. Derivatives of DPA were then synthesized and IC_{50} values were determined with a wider range of FBP aldolases. IC_{50} values are generally similar with DPA and compound **1**, which differs from DPA by the substitution of the carboxylate with a phosphomethyl group at the 6-position of the pyridine ring. Addition of other substituents (in compounds **2** to **6**) resulted in higher IC_{50} values for most enzymes. Two exceptions are compounds **5** and **6**, respectively with hydroxymethyl and formyl substituents in position 4 of the pyridine ring, which had IC_{50}s comparable to DPA and compound **1** with the *M. tuberculosis* aldolase. The generally poorer inhibition observed with compounds **2** to **4** in *M. tuberculosis* aldolase initially did not appear to be due to steric hindrance in the active site of the enzyme since compound **7**, with a 3,5-dicarboxyphenyl substituent in position 4 of the pyridine ring was found to be better than DPA in inhibiting this enzyme (Table 2). However, molecular modeling revealed that the substituents in position 3 and 4 of the pyridine ring of compounds **2** and **3** make unfavorable contacts with key active site residues, unlike compound **1**. The improved inhibition obtained with compound **7** could be the result of favorable interactions of its dicarboxyphenyl substituent with GAP binding residues located in the adjacent dimer subunit [5]. The fact that compound **7** partially inhibits the Class I FBP aldolase reaction at high concentration (Section 3.2) also suggests that this compound may be closer to an FBP analog than the other metal-chelating compounds.

Upon further kinetic analyses, it was noticed that the inhibition by these compounds was weaker in the presence of the FBP substrate, implying a competitive mechanism. A time-dependent analysis of reaction progress curves of the cleavage of FBP by the *M. tuberculosis* aldolase in the presence of the most potent inhibitors showed that compounds **1**, **7**, and DMPS were better competitive inhibitors than DPA, according to their second order binding rate constants. EDTA was comparatively a weak inhibitor of the enzyme in the presence of substrate, being 6 times less potent than DPA. The first-order apparent rate constant for inhibition of FBP cleavage (*k*, or A[I] in Eqs. (1) and (2)) were dependent on the concentration of the inhibitors EDTA, DPA, compound **1**, Compound **7** and DMPS (over the concentration range 25 μM–500 μM inhibitor), confirming that the inhibition mechanism involves the formation of a ternary complex [36] (Fig. 4).

In our study, the enzymes were reactivated by the addition of small amounts of zinc (i.e. ~10 times less zinc than the inhibitor concentration), which indicates that the inhibitors are forming an unstable ternary complex with the active site and the zinc ion. The DPA derivatives tested therefore do not have a sufficient affinity for the active site to form a stable complex in the presence of extraneous zinc. In contrast, the inhibitor PGH was shown to form a stable complex with the cobalt-dependant *Bacillus stearothermophilus* Class II FBP aldolase, as the inhibited enzyme was not reactivated in the presence of excess cobalt [37]. Our data however shows that some chelating inhibitors, such as DMPS and compound **1**, are better able to compete with the substrate FBP for the access to the active site zinc in the *M. tuberculosis* aldolase in comparison with DPA or EDTA, which means that some of the studied compounds have a higher affinity for the active site than others.

The *in silico* docking studies indicate that the DPA derivatives cannot form bidentate bonds with the zinc ion while it remains in its catalytic location, due to both the restricted size and geometry of the DHAP binding pocket, where the zinc ion is located; and the limited solvent-exposed surface of the catalytic metal. This is in agreement with the conclusions of a recent report on the inhibition of the *G. lamblia* Class II FBP aldolase by metal-chelating aromatic compounds [38]. The authors found that the orientation of a 3-hydroxy-2-pyridone ligand in the binding pocket was not consistent with strong bonds with the active site zinc in the crystal structure. They concluded the zinc stabilizes the reaction intermediate (enediolate form of DHAP), but does not provide significant binding energy in the enzyme-substrate complex [38].

It appears that the presence of a substrate analog in the active site is necessary to induce conformational changes in Class II FBP aldolases that cause the zinc ion to move from a buried location to a solvent-exposed position, which then allows strong interactions between the zinc ion and the enzyme substrates/inhibitors [38–41]. The slow inhibition observed with the metal-chelating compounds may be related to the buried location of the catalytic zinc in the absence of substrate. In our study, molecular modeling results confirmed that most interactions between the metal-chelating inhibitors and the enzyme active site involve the phosphate binding pocket residues. However, these results also show that some inhibitors can alter the catalytic zinc environment. It is relevant to point out that in some minimized models of *M. tuberculosis* aldolase with the chelating inhibitors, the interaction of the catalytic zinc with its ligand His_{212} is considerably weakened compared to the interaction seen in the original crystal structure (Fig. 5A). This weakened interaction with His_{212} is concomitant with the new interaction of the carboxylate group of Asp_{95} with the catalytic zinc mentioned in Section 3.3. This is the case for the minimized models with DPA, Compounds **4**, **5** and **6** (Figs. 5C and C2A-C2C), as well as *R*-DMPS,

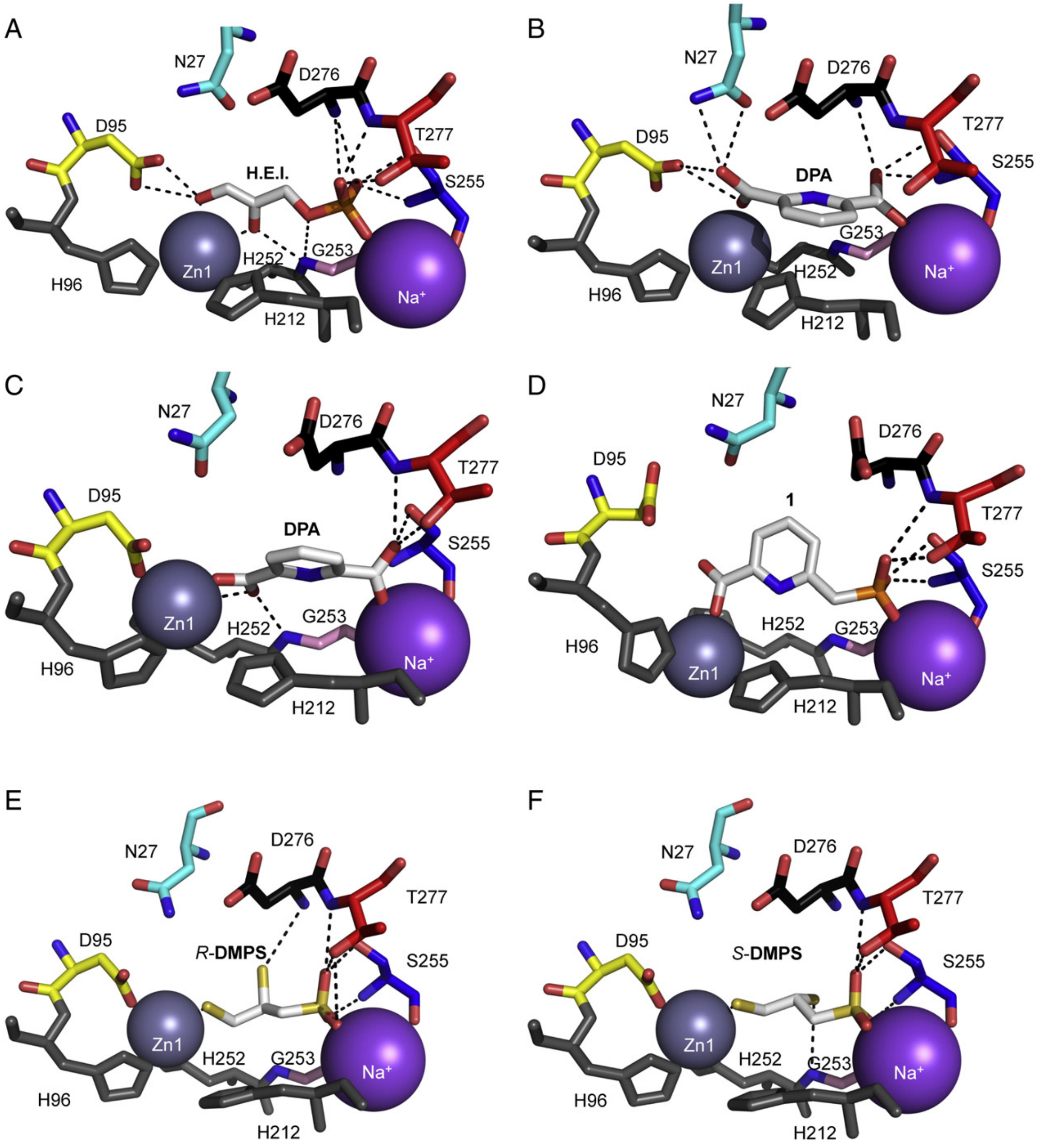
A
N27
D276
D95
H.E.I.
T277
S255
G253
H252
Zn1
H96
Na+
H212
B
N27
D276
D95
DPA
T277
S255
G253
Zn1
H252
H96
Na+
H212
C
N27
D276
T277
D95
DPA
S255
Zn1
H252
G253
H96
Na+
H212
D
N27
D276
D95
1
T277
S255
H96
H252
G253
Zn1
Na+
H212
E
N27
D276
T277
D95
R-DMPS
S255
Zn1
H252
G253
Na+
H96
H212
F
N27
D276
T277
D95
S-DMPS
S255
Zn1
H252
G253
Na+
H96
H212

Fig. 5. *M. tuberculosis* FBP aldolase (PDB ID 3EKZ) with substrate DHAP (High Energy Intermediate) and modeled inhibitors. The DHAP enediolate form (High Energy Intermediare) and the docked compounds are represented as sticks with carbons in white, oxygens in red, nitrogen in blue, sulfur in yellow, and phosphorus in orange. The active site residues are shown as sticks with colored carbon aroms: D95 in yellow, N27 in cyan, S255 in blue, D276 in black, T277 in red, G253 in pink. The zinc ligands H96, H212 and H252 are shown as gray sticks. The catalytic zinc (Zn1) is represented as a gray sphere (bottom left) and the Na^+ is represented as a purple sphere (right). The electrostatic interactions between 2 and 3.6 Å are shown as black dashes. A) DHAP High Energy Intermediate (H.E.I.); B) docked DPA; C) to F) DPA, compound **1** *R*-DMPS, and *S*-DMPS minimized using the anneal function of Sybyl (Tripos, St. Louis, MO). The figures were produced using PyMOL (DeLano Scientific LLC).

and *S*-DMPS (Fig. 5E and F). It is possible that this zinc ligand exchange in the presence of the inhibitors constitutes the first step of a slow ligand exchange process, which could lead to a bidentate interaction of the metal ion with the chelating inhibitors as the zinc leaves its catalytic location. This could possibly lead to the removal of the catalytic zinc from the enzyme when the metal-inhibitor complex leaves the active site. These modeling results are also consistent with previous reports of the considerable mobility of the catalytic zinc in Class II FBP aldolases [35–38].

5. Conclusions

The strongest inhibitors in our study according to the second order binding rate constants (k_{on}) were DMPS and compound **1**, which respectively possess a sulfonate and a phosphonate group in addition to zinc-chelating functions. Molecular modeling results suggest that the strongest interaction between these compounds and the enzyme occurs via the phosphate binding pocket ligands. Molecular modeling results also suggest that the compounds cannot bind the catalytic zinc ion in a bidentate fashion while the metal is chelated by the active site zinc ligands, but indicate that several inhibitors can alter the zinc environment. In order to eliminate the possibility of zinc removal from the enzyme, the first generation inhibitory compounds produced in this study could be modified by the addition of R-groups extending out of the FBP binding pocket to promote stronger interactions and improved specificity for the Class II FBP aldolase from different pathogens. Longer-chain FBP analogues containing metal-chelating functions have been shown recently to be very potent inhibitors of the *S. cerevisiae*, *C. albicans*, *H. pylori*, *M. tuberculosis, M. bovis* and *Y. pestis* Class II aldolases [18,21]. The use of metal-chelating substrate analogues, like the ones reported in the present study, is therefore very promising for the development of new drugs targeting the Class II FBP aldolase.

6. Abbreviations

BSA	bovine serum albumin
DHAP	dihydroxyacetone phosphate
DMPS	2,3-dimercaptopropane-1-sulfonate
DPA	dipicolinic acid
FBP	Fructose 1,6-bisphosphate
GAP	glyceraldehyde-3-phosphate
H.E.I.	High Energy Intermediate (enediolate form of DHAP)
PGH	phosphoglycolohydroxamic acid

Acknowledgements

G.L. is the grateful recipient of an Ontario Graduate Scholarship, a UW President's Graduate Scholarship, and a UW Provost's/Faculty of Science Graduate Women's Incentive Fund. This research was supported by the Natural Science and Engineering Research Council of Canada Grants 18351, 927-2008 and 235003.

Appendix A. Supplementary data

Supplementary data to this article can be found online at doi:10.1016/j.jinorgbio.2012.02.032.

References

[1] D.J. Lewis, G. Lowe, J. Chem. Soc. Chem. Commun. (1973) 713–715.

[2] T. Baba, T. Ara, M. Hasegawa, Y. Takai, Y. Okumura, M. Baba, K.A. Datsenko, M. Tomita, B.L. Wanner, H. Mori, Mol. Syst. Biol. 2 (2006) 2006.0008.

[3] G. Lamichhane, M. Zignol, N.J. Blades, D.E. Geiman, A. Dougherty, J. Grosset, K.W. Broman, W.R. Bishai, Proc. Natl. Acad. Sci. U. S. A. 100 (2003) 7213–7218.

[4] N.T. Liberati, J.M. Urbach, S. Miyata, D.G. Lee, E. Drenkard, G. Wu, J. Villanueva, T. Wei, F.M. Ausubel, Proc. Natl. Acad. Sci. U. S. A. 103 (2006) 2833–2838.

[5] S.D. Pegan, K. Rukseree, S.G. Franzblau, A.D. Mesecar, J. Mol. Biol. 386 (2009) 1038–1053.

[6] J.H. Song, K.S. Ko, J.Y. Lee, J.Y. Baek, W.S. Oh, H.S. Yoon, J.Y. Jeong, J. Chun, Mol. Cells 19 (2005) 365–374.

[7] A. Rodaki, T. Young, A.J. Brown, Eukaryot. Cell 5 (2006) 1371–1377.

[8] S.Y. Gerdes, M.D. Scholle, J.W. Campbell, G. Balazsi, E. Ravasz, M.D. Daugherty, A.L. Somera, N.C. Kyrpides, I. Anderson, M.S. Gelfand, A. Bhattacharya, V. Kapatral, M. D'Souza, M.V. Baev, Y. Grechkin, F. Mseeh, M.Y. Fonstein, R. Overbeek, A.L. Barabasi, Z.N. Oltvai, A.L. Osterman, J. Bacteriol. 185 (2003) 5673–5684.

[9] G. Giaever, A.M. Chu, L. Ni, C. Connelly, L. Riles, S. Veronneau, S. Dow, A. Lucau-Danila, K. Anderson, B. Andre, A.P. Arkin, A. Astromoff, M. El Bakkoury, R. Bangham, R. Benito, S. Brachat, S. Campanaro, M. Curtiss, K. Davis, A. Deutschbauer, K.D. Entian, P. Flaherty, F. Foury, D.J. Garfinkel, M. Gerstein, D. Gotte, U. Guldener, J.H. Hegemann, S. Hempel, Z. Herman, D.F. Jaramillo, D.E. Kelly, S.L. Kelly, P. Kotter, D. LaBonte, D.C. Lamb, N. Lan, H. Liang, H. Liao, L. Liu, C. Luo, M. Lussier, R. Mao, P. Menard, S.L. Ooi, J.L. Revuelta, C.J. Roberts, M. Rose, P. Ross-Macdonald, B. Scherens, G. Schimmack, B. Shafer, D.D. Shoemaker, S. Sookhai-Mahadeo, R.K. Storms, J.N. Strathern, G. Valle, M. Voet, G. Volckaert, C.Y. Wang, T.R. Ward, J. Wilhelmy, E.A. Winzeler, Y. Yang, G. Yen, E. Youngman, K. Yu, H. Bussey, J.D. Boeke, M. Snyder, P. Philippsen, R.W. Davis, M. Johnston, Nature 418 (2002) 387–391.

[10] M.A. Jacobs, A. Alwood, I. Thaipisuttikul, D. Spencer, E. Haugen, S. Ernst, O. Will, R. Kaul, C. Raymond, R. Levy, L. Chun-Rong, D. Guenthner, D. Bovee, M.V. Olson, C. Manoil, Proc. Natl. Acad. Sci. U. S. A. 100 (2003) 14339–14344.

[11] K. Kobayashi, S.D. Ehrlich, A. Albertini, G. Amati, K.K. Andersen, M. Arnaud, K. Asai, S. Ashikaga, S. Aymerich, P. Bessieres, F. Boland, S.C. Brignell, S. Bron, K. Bunai, J. Chapuis, L.C. Christiansen, A. Danchin, M. Debarbouille, E. Dervyn, E. Deuerling, K. Devine, S.K. Devine, O. Dreesen, J. Errington, S. Fillinger, S.J. Foster, Y. Fujita, A. Galizzi, R. Gardan, C. Eschevins, T. Fukushima, K. Haga, C.R. Harwood, M. Hecker, D. Hosoya, M.F. Hullo, H. Kakeshita, D. Karamata, Y. Kasahara, F. Kawamura, K. Koga, P. Koski, R. Kuwana, D. Imamura, M. Ishimaru, S. Ishikawa, I. Ishio, D. Le Coq, A. Masson, C. Mauel, R. Meima, R.P. Mellado, A. Moir, S. Moriya, E. Nagakawa, H. Nanamiya, S. Nakai, P. Nygaard, M. Ogura, T. Ohanan, M. O'Reilly, M. O'Rourke, Z. Pragai, H.M. Pooley, G. Rapoport, J.P. Rawlins, L.A. Rivas, C. Rivolta, A. Sadaie, Y. Sadaie, M. Sarvas, T. Sato, H.H. Saxild, E. Scanlan, W. Schumann, J.F. Seegers, J. Sekiguchi, A. Sekowska, S.J. Seror, M. Simon, P. Stragier, R. Studer, H. Takamatsu, T. Tanaka, M. Takeuchi, H.B. Thomaides, V. Vagner, J.M. van Dijl, K. Watabe, A. Wipat, H. Yamamoto, M. Yamamoto, Y. Yamamoto, K. Yamane, K. Yata, K. Yoshida, H. Yoshikawa, U. Zuber, N. Ogasawara, Proc. Natl. Acad. Sci. U. S. A. 100 (2003) 4678–4683.

[12] C.M. Sassetti, D.H. Boyd, E.J. Rubin, Mol. Microbiol. 48 (2003) 77–84.

[13] U.F. Wehmeier, FEMS Microbiol. Lett. 197 (2001) 53–58.

[14] M. de la Paz Santangelo, P.M. Gest, M.E. Guerin, M. Coincon, H. Pham, G. Ryan, S.E. Puckett, J.S. Spencer, M. Gonzalez-Juarrero, R. Daher, A.J. Lenaerts, D. Schnappinger, M. Therisod, S. Ehrt, J. Sygusch, M. Jackson, J. Biol. Chem. 286 (2011) 40219–40231.

[15] A. Bock, F.C. Neidhardt, J. Bacteriol. 92 (1966) 470–476.

[16] D.A. Schneider, R.L. Gourse, J. Bacteriol. 185 (2003) 6192–6194.

[17] C.H. Su, J.P. Merlie, H. Goldfine, J. Bacteriol. 122 (1975) 565–569.

[18] M. Fonvielle, M. Coincon, R. Daher, N. Desbenoit, K. Kosieradzka, N. Barilone, B. Gicquel, J. Sygusch, M. Jackson, M. Therisod, Chemistry 14 (2008) 8521–8529.

[19] M. Fonvielle, P. Weber, K. Dabkowska, M. Therisod, Bioorg. Med. Chem. Lett. 14 (2004) 2923–2926.

[20] S. Gavalda, R. Braga, C. Dax, A. Vigroux, C. Blonski, Bioorg. Med. Chem. Lett. 15 (2005) 5375–5377.

[21] R. Daher, M. Coincon, M. Fonvielle, P.M. Gest, M.E. Guerin, M. Jackson, J. Sygusch, M. Therisod, J. Med. Chem. 53 (2010) 7836–7842.

[22] G. Rosenblum, S.O. Meroueh, O. Kleifeld, S. Brown, S.P. Singson, R. Fridman, S. Mobashery, I. Sagi, J. Biol. Chem. 278 (2003) 27009–27015.

[23] A.T. Colak, F. Colak, O.Z. Yesilel, O. Buyukgungor, J. Mol. Struct. 936 (2009) 67–74.

[24] Y. Kidani, J. Hirose, H. Koike, J. Biochem. 79 (1976) 43–51.

[25] Y. Kidani, J. Hirose, J. Biochem. 81 (1977) 1383–1391.

[26] Y. Pocker, C.T. Fong, Biochemistry 19 (1980) 2045–2050.

[27] G. Labbe, J. Bezaire, S.d. Groot, C. How, T. Rasmusson, J. Yaeck, E. Jervis, G.I. Dmitrienko, J. Guy Guillemette, Protein Expr. Purif. 51 (2007) 110–119.

[28] P.C. Ramsaywak, G. Labbe, S. Siemann, G.I. Dmitrienko, J.G. Guillemette, Protein Expr. Purif. 37 (2004) 220–228.

[29] G. Labbe, S. de Groot, T. Rasmusson, G. Milojevic, G.I. Dmitrienko, J.G. Guillemette, Protein Expr. Purif. 80 (2011) 224–233.

[30] J.F. Morrison, C.T. Walsh, Adv. Enzymol. Relat. Areas Mol. Biol. 61 (1988) 201–301.

[31] C.L. Tsou, Adv. Enzymol. Relat. Areas Mol. Biol. 61 (1988) 381–436.

[32] O. Trott, A.J. Olson, J. Comput. Chem. 31 (2010) 455–461.

[33] G.M. Morris, R. Huey, W. Lindstrom, M.F. Sanner, R.K. Belew, D.S. Goodsell, A.J. Olson, J. Comput. Chem. 30 (2009) 2785–2791.

[34] X. Hu, W.H. Shelver, J. Mol. Graph. Model. 22 (2003) 115–126.

[35] S. Siemann, A.J. Clarke, T. Viswanatha, G.I. Dmitrienko, Biochemistry 42 (2003) 1673–1683.

[36] D.S. Auld, Methods Enzymol. 248 (1995) 228–242.

[37] D.J. Lewis, G. Lowe, Eur. J. Biochem. 80 (1977) 119–133.

[38] Z. Li, Z. Liu, D.W. Cho, J. Zou, M. Gong, R.M. Breece, A. Galkin, L. Li, H. Zhao, G.D. Maestas, D.L. Tierney, O. Herzberg, D. Dunaway-Mariano, P.S. Mariano, J. Inorg. Biochem. 105 (2010) 509–517.

[39] N.S. Blom, S. Tetreault, R. Coulombe, J. Sygusch, Nat. Struct. Biol. 3 (1996) 856–862.

[40] T. Izard, J. Sygusch, J. Biol. Chem. 279 (2004) 11825–11833.

[41] D.R. Hall, L.E. Kemp, G.A. Leonard, K. Marshall, A. Berry, W.N. Hunter, Acta Crystallogr. D: Biol. Crystallogr. 59 (2003) 611–614.

[42] M. St-Jean, C. Blonski, J. Sygusch, Biochemistry 48 (2009) 4528–4537.